Magphan® RT

Extended Field of View, Easy-to-handle Design

An integrated system designed for radiotherapy specific MR Image QA

The growing use of MRI for radiation therapy holds great promise for improved treatment accuracy and, ultimately, patient outcomes. However, radiotherapy applications demand much greater spatial accuracy and uniform response across an extended field-of-view.

Magphan RT combines a unique, easy-to-handle phantom design with intuitive and accurate analysis from Image Owl to accurately characterize radiotherapy critical parameters.

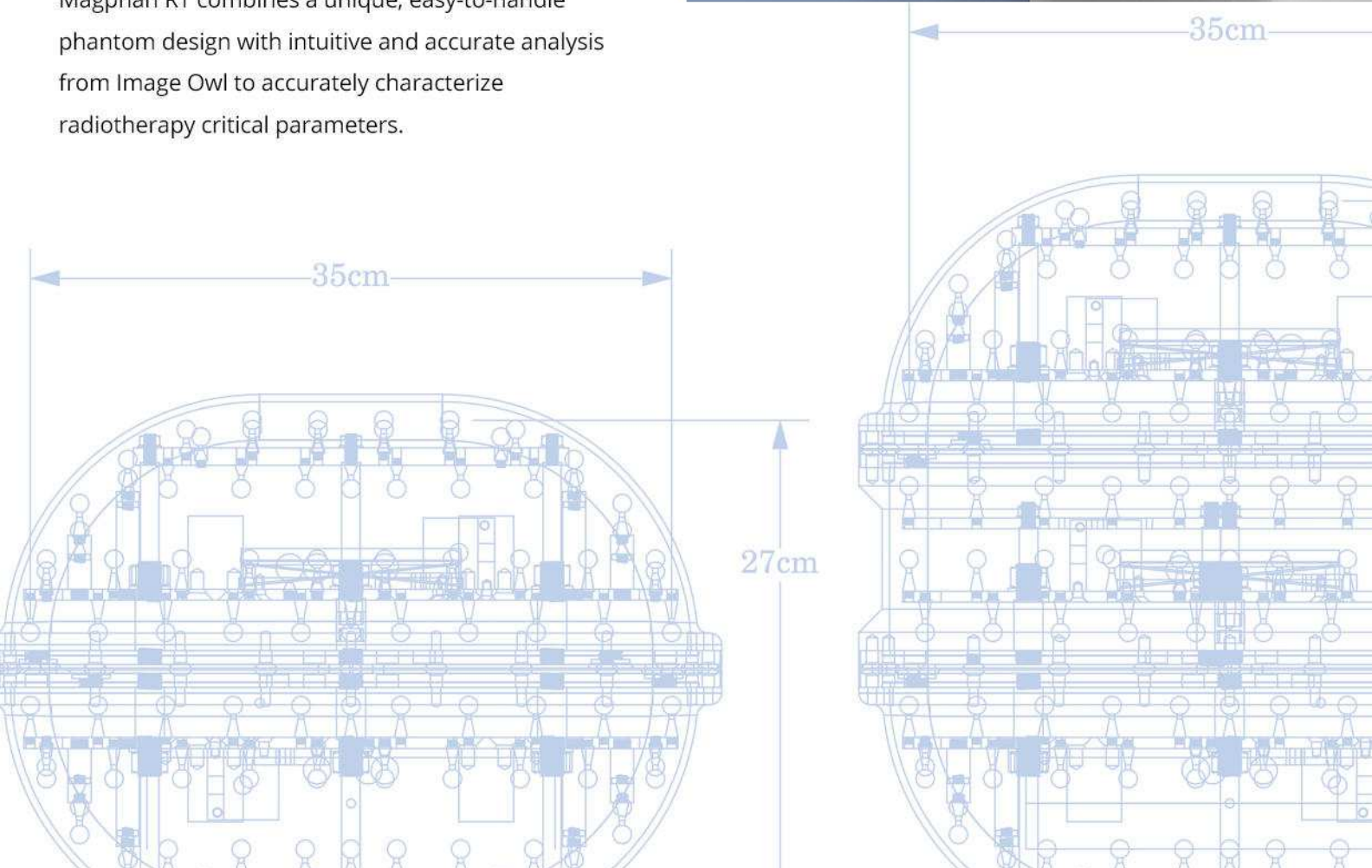

The effects of iterative reconstruction and kernel selection on quantitative computed tomography measures of lung density

Alfonso Rodriguez
Department of Medical Physics, University of Wisconsin School of Medicine and Public Health, Madison, WI, USA

Frank N. Ranallo
Department of Medical Physics, University of Wisconsin School of Medicine and Public Health, Madison, WI, USA
Department of Radiology, University of Wisconsin School of Medicine and Public Health, Madison, WI, USA

Philip F. Judy
Brigham and Women's Hospital, Boston, MA, USA

Sean B. Fain[a)]
Department of Medical Physics, University of Wisconsin School of Medicine and Public Health, Madison, WI, USA
Department of Radiology, University of Wisconsin School of Medicine and Public Health, Madison, WI, USA
Department of Biomedical Engineering, University of Wisconsin School of Engineering, Madison, WI, USA

(Received 5 August 2016; revised 23 January 2017; accepted for publication 8 February 2017; published 12 May 2017)

Purpose: To determine the effects of iterative reconstruction (IR) and high-frequency kernels on quantitative computed tomography (qCT) density measures at reduced X-ray dose.
Materials and methods: The COPDGene 2 Phantom (CTP 698, The Phantom Laboratory, Salem, NY) with four embedded lung mimicking foam densities (12lb, 20lb, and 4lb), as well as water, air, and acrylic reference inserts, was imaged using a GE 64 slice CT750 HD scanner in helical mode with four current-time products ranging from 12 to 100 mAs. The raw acquired data were reconstructed using standard (STD — low frequency) and Bone (high frequency) kernels with filtered back projection (FBP), 100% ASiR, and Veo reconstruction algorithms. The reference density inserts were manually segmented using Slicer3D (www.slicer.org), and the mean, standard deviation, and histograms of the segmented regions were generated using Fiji (http://fiji.sc/Fiji) for each reconstruction. Measurements of threshold values placed on the cumulative frequency distribution of voxels determined by these measured histograms at 5%, $PD5_{phant}$, and 15%, $PD15_{phant}$, (analogous to the relative area below −950 HU (RA-950) and percent density 15 (PD15) in human lung emphysema quantification, respectively), were also performed.
Results: The use of high-resolution kernels in conjunction with ASiR and Veo did not significantly affect the mean Hounsfield units (HU) of each of the density standards (< 4 HU deviation) and current-time products within the phantom when compared with the STD+FBP reconstruction conventionally used in clinical applications. A truncation of the scanner reported HU values at −1024 that shifts the mean toward more positive values was found to cause a systematic error in lower attenuating regions. Use of IR drove convergence toward the mean of measured histograms (~100–137% increase in the number measured voxels at the mean of the histogram), while the combination of Bone+ASiR preserved the standard deviation of HU values about the mean compared to STD+FBP, with the added effect of improved spatial resolution and accuracy in airway measures. $PD5_{phant}$ and $PD15_{phant}$ were most similar between the Bone+ASiR and STD+FBP in all regions except those affected by the −1024 truncation artifact.
Conclusions: Extension of the scanner reportable HU values below the present limit of −1024 will mitigate discrepancies found in qCT lung densitometry in low-density regions. The density histogram became more sharply peaked, and standard deviation was reduced for IR, directly effecting density thresholds, $PD5_{phant}$ and $PD15_{phant,}$ placed on the cumulative frequency distribution of each region in the phantom, which serve as analogs to RA-950 and PD15 typically used in lung density quantitation. The combination of high-frequency kernels (Bone) with ASiR mitigates this effect and preserves density measures derived from the image histogram. Moreover, previous studies have shown improved accuracy of qCT airway measures of wall thickness (WT) and wall area percentage (WA%) when using high-frequency kernels in combination with ASiR to better represent airway walls. The results therefore suggest an IR approach for accurate assessment of airway and parenchymal density measures in the lungs. [https://doi.org/10.1002/mp.12255]

Key words: computed tomography, emphysema, iterative reconstruction, lung density, perc15, quantitative imaging, RA950

1. INTRODUCTION

The regional characterization of obstructive lung disease (OLD) such as chronic obstructive pulmonary disease (COPD) and asthma using high-resolution computed tomography (HRCT) for assessment of lung structure is of increasing interest with the latest innovations of multislice CT scanners.[1–4] Larger detector configurations (32, 64, and 128 slice detector banks) allow for entire volume acquisitions in reduced acquisition times to minimize motion artifacts. This has enabled high-resolution images for quantitative measurement of pulmonary structures such as the airways and lung parenchymal density to characterize longitudinal progression of disease in OLD.[5–9] CT lung density measures have the potential of being both more sensitive and specific for assessment of lung impairment via emphysema over currently used spirometric lung function tests.[10] Currently, biomarkers derived from the histogram of the voxel values in segmented lung CT images have been correlated to morphology and severity of disease in OLD.[10,11] Parenchymal density measures serve as an estimate of the severity of emphysema, and air trapping in patients of OLD. Two such biomarkers of emphysema include the relative area under the curve of the histogram of the lung for inspiratory CT acquisitions, which fall below −950 HU (RA-950), and the HU threshold of the lower 15% of the histogram distribution (PD15 also termed "Perc15").[10,11] Measures of central airway morphology, such as airway wall thickening and lumen area, are also important biomarkers of airway remodeling in OLD, both for COPD[12,13] and for asthma.[14,15]

However, there are growing concerns over the use of CT for longitudinal studies due to ionizing radiation burden. Currently, CT is the major contributor to medical sources of ionizing radiation worldwide and has raised some concerns among the medical community from increased likelihood of development of malignancies from patients who require imaging as part of treatment.[16] Thus, the focus of current use of quantitative CT (qCT) is to reduce the dose of ionizing radiation to patients, while maintaining qualitative and quantitative diagnostic quality for longitudinal pulmonary imaging studies. Unfortunately parameters such as reconstruction slice thickness, acquisition dose, and selection of reconstruction kernel have been shown to have significant effects on qCT measures of lung parenchymal density[10,17,18] and airway morphology.[19] In addition to reduced CT dose, the use of a sharper reconstruction kernel has been shown to overestimate emphysema severity due to a relative flattening of the lung histogram from increased noise.[10,17,20,21] This has led to the general recommendation to use softer kernels such as GE's standard or detail kernel as opposed to sharper, high-frequency kernels such as GE's Bone kernel and often with thicker slices of about 3 to 5 mm to further reduce noise.[21]

New iterative reconstruction (IR) methods offer a strategy to reduce dose in qCT while mitigating the noise penalty from fewer photon counts. Statistical IR methods to reduce noise vary by manufacturer, but typically use an initial filtered back projection (FBP) reconstruction as a starting point, and iteratively reduce pixel variance based on estimates of image noise derived from stochastic fluctuations within projection data. Examples include Sinogram Affirmed IR (SAFIRE, Siemens), Adaptive Statistical IR (ASiR, General Electric), and Adaptive Iterative Dose Reduction (AIDR, Toshiba) techniques. Model-based IR (MBIR) techniques, such as Siemens' Advanced Modeled Iterative Reconstruction (ADMIRE) and General Electric's (GE) Veo, are the latest innovations in IR and rely heavily on proper modeling of the source beam and other CT parameters during the reconstruction process rather than strictly stochastic variations.

Studies have shown that IR, in general, can greatly reduce image noise in lower dose CT acquisitions to produce diagnostic quality images.[22–25] Moreover, a similar study of quantitative CT density measurements has shown that there is no significant effect on mean Hounsfield units (HU).[26] However, IR has the effect of decreasing noise leading to a more "peaked," less flat, histogram of the lung densities emphasizing the need for careful study before its use in qCT to evaluate emphysema in patients.[22,27,28]

This study investigates the impact of IR, reconstruction kernel, and the combination of the two on qCT measures of the density histogram. The effects of higher resolution kernels in conjunction with both statistical and model-based IR on the density histogram can be investigated using reference foam inserts of various densities similar to tissues and structures found in the human lung in a published phantom (COPDGene 2).[14] The COPD Gene 2 phantom allows for repeated scans at progressively lower scan doses to further test the feasibility of using IR for qCT density measures in low dose protocols. This analysis is motivated in part by our previous finding that the use of the Bone kernel together with ASiR at half display field of view (DFOV) showed improved accuracy (by a factor of 50% in some cases) for airway measures such as wall thickness (WT) and wall area percentage (WA%).[19,29] Moreover, in the same study, accuracy was maintained down to one-fourth the dose of a conventional dose reference protocol. The current work extends this approach to evaluate impacts on qCT measurement of lung parenchymal density.

2. METHODS

2.A. CT scanning and reconstruction

In this study, a GE CT750 HD Discovery 64 slice scanner was used to obtain images of the test object. The software

version installed on the scanner was able to reconstruct images with FBP, ASiR with varying percentages from 0 to 100%, and Veo reconstruction algorithms. Images of the COPDgene phantom were obtained using helical mode on the CT750 at tube currents of 200, 100, 50, and 25 mA (corresponding to CTDIvol values of 7.44, 3.72, 1.86, and 0.93 mGy, respectively); tube potential of 120 kV, beam collimation of 40 mm, pitch of 0.984, gantry rotation speed of 0.5 s, and 0.625 mm slice thickness. The parameters detailed here correspond to a standard CT acquisition at 200 mA (100 mAs) for ongoing qCT imaging studies of lung disease in asthma (Severe Asthma Research Program and COPDgene) with decreasing fractions of this CT dose down to 25 mA (12.5 mAs). Following the helical acquisitions, the scan data were then reconstructed at a slice spacing of 0.5 mm, using GE's standard and Bone reconstruction kernels with FBP, 100% ASiR and Veo reconstruction algorithms, although it must be noted that kernel selection was not available for Veo recons on our scanner software version (SW Release 10MW25.6). While the only parameter reported by the software for the Veo recon in this study was the slice thickness of 0.625 mm, we were able to verify that the standard kernel was the default.[30] Also from our previous studies, the combination of Bone+FBP for image reconstruction was excluded from the testing scheme since at lower doses, < 100 mAs, the noise in the image increased dramatically to diagnostically unacceptable levels. In addition, recommendations from other studies make a point to avoid using bone kernel with FBP for fear of overestimating emphysema.[10,17,19–21] The acquisition and reconstruction parameters for this study are summarized in Table I.

2.B. Test object, and analysis tools

The test object in our experiment was the COPDGene Study Quality Assurance Phantom (CTP698; The Phantom Laboratory, Schenectady, NY, USA) which contains several material inserts embedded in a lung equivalent density foam shown in Fig. 1, including three reference foams with density similar to tissues typically found in the lung, an air cavity, water bottle and polycarbonate plastic tubes of known dimensions used in previous work to assess airway measure accuracy.[19] To better simulate patient scatter conditions, the COPDGene2 phantom was bookended by additional 7.5 cm thick water attenuating phantoms. In total, the combined axial extent of the configuration of phantoms was 20 cm in length. The focus of our investigation was the seven different materials (numbered I-VII in Fig. 1) most of which were 5 cm in length and 3 cm in diameter. These homogenous cylinders included; I: 20 lb reference foam (−824 HU), II: water (0 HU), III: 12 lb reference foam (−703 HU), IV: acrylic (120 HU), V: 4 lb reference foam (−937 HU), VI: air (−1000 HU). The lung equivalent foam (VII with −856 HU) was the larger 25 cm wide, 15 cm high, and 5 cm thick background into which the rest of the materials were embedded in the phantom. Also, it should be noted that the water region in the experiment was contained in a bottle that was slightly smaller than the other cylindrical inserts with a diameter of 3 cm and a length of ~3.5 cm. This specific selection of materials and their associated densities in the phantom corresponds to the range of electron densities typically found in quantitative CT studies of the lung.

Using the acquired CT images of the COPDGene 2 phantom, histograms of each of the different materials was generated via manually segmented regions using *3DSlicer* (www.slicer.org), software version 4.40.[31] The "volume clip with ROI" tool in *3DSlicer* was used to segment each material detailed above. The resulting volume was further eroded by four voxels to minimize

TABLE I. A summary of the acquisition and reconstruction parameters used to image the COPDGene 2 phantom. Kernels included a softer low frequency kernel (Standard) and a high-frequency kernel (Bone). 100% ASiR was used to focus on the IR effect of the recon and avoid mixing with FBP.

CT scan parameters	
Tube voltage, kV	120
Scan type	Helical
Rotation time, s	0.5
Collimation, mm	64 × 0.625
Pitch	0.984
Slice thickness, mm	0.625
Matrix	512 × 512
Recon option	Plus; IQ enhance: OFF
Recon kernel	Standard, Bone
Recon algorithm	FBP, 100% ASiR, Veo

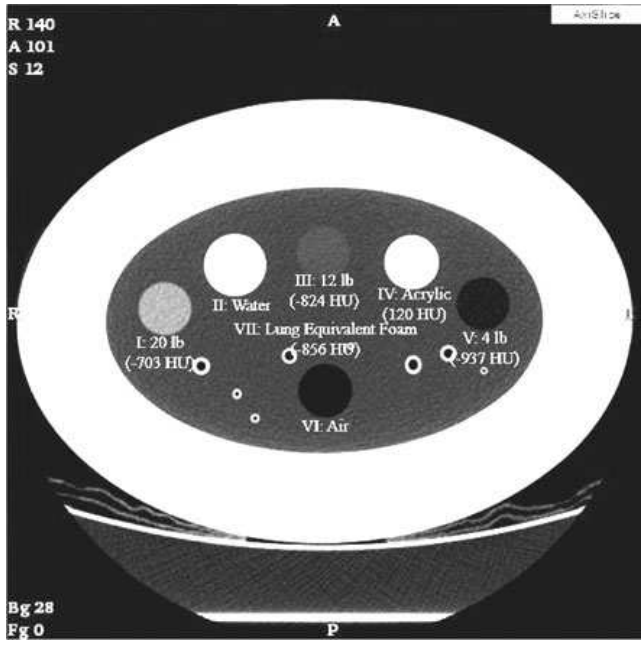

FIG. 1. An image of the COPDGene2 phantom with a variety of density inserts, shown as the larger cylindrical plugs, which are labeled I-VII; I: 20 lb reference foam (−824 HU), II: water, III: 12 lb reference foam (−703 HU), IV: acrylic (120 HU), V: 4 lb reference foam (−937 HU), VI: air, and VII: lung equivalent foam (−856 HU).

partial volume effects at the edges of the volume. A box-shaped ROI of dimensions 2 cm wide by 2 cm high by 4.2 cm long in the axial dimension was defined in the volume clip tool and placed in the center of each of the cylindrical inserts, including the center of the lung equivalent foam (VII in Fig. 1) to perform the manual segmentation as is shown in Fig. 2(a). The ROI was shortened in the axial direction by 1.3 cm when measuring the water region due its smaller size. The "Simple Region Growing Segmentation" tool was also used to segment the lung (Fig. 2(b)) for the experiment on a sample human lung segmentation detailed further in Section C below. The resulting segmentations obtained in *Slicer3D* were then analyzed using *FIJI* (http://fiji.sc/Fiji) to generate the histograms as well as the mean and standard deviation (σ_{HU}) of the distribution of voxel values. *Matlab* (The Mathworks Inc., Natick, MA, USA) was used to fit model Gaussian curves to the resulting histograms.

2.C. Exemplary histograms: "Statement of the Problem"

For illustrative purposes, two image histograms and their corresponding density measures are shown in Fig. 3; the histograms demonstrate the impact of noise amplification on the density histogram that occurs when using the Bone+FBP combination for reconstruction and further corroborates findings by Shaker, et al.[21] Raw data from a human subject scan were reconstructed retrospectively with FBP using both a standard and Bone kernel, and the resulting lung histograms were plotted on the same graph. The general flattening effect of using the sharper kernel does not significantly affect the mean HU value of the distribution, but the threshold measures such as RA-950 and PD15 change substantially between the two reconstructions and may explain the overestimation of emphysema scores often observed in previous studies. Both RA-950 (hashed area in Fig. 3) and PD15 measures (solid and dotted vertical arrows in Fig. 3) of the histogram

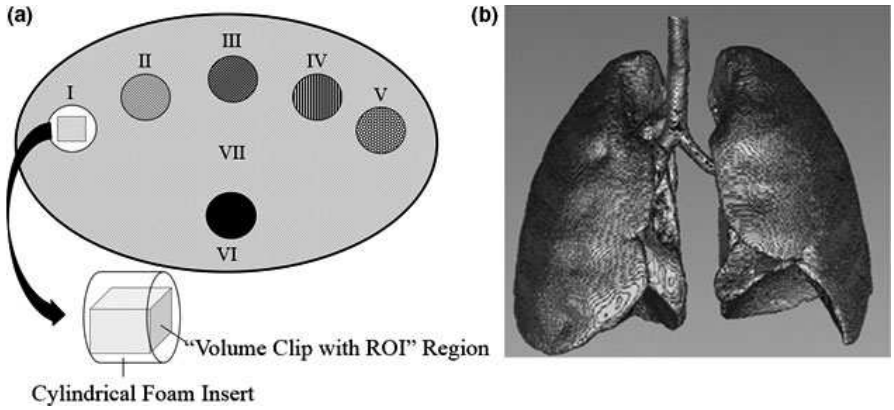

FIG. 2. (a) A schematic of the "volume clip with ROI" tool in Slicer3D that was positioned within each of the regions of the phantom. (b) A volume render of the segmented lung using the "simple region growing segmentation" tool excluding the low-density lumen regions of the airways.

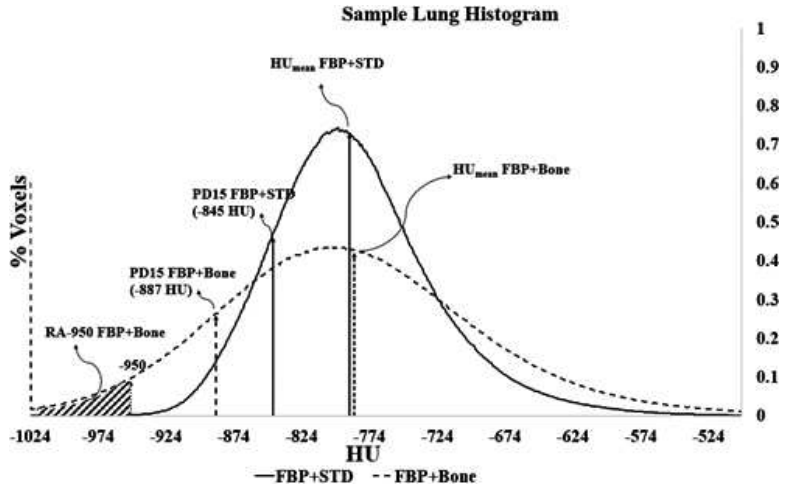

FIG. 3. A sample lung density histogram from a human subject reconstructed with FBP using both standard (solid) and bone (dashed) kernels with the −950 HU location depicted as a vertical dotted line. The mean does not vary much between the two reconstructions, but the RA-950 (hashed area) and PD15 (dashed vs. solid vertical arrows) change substantially.

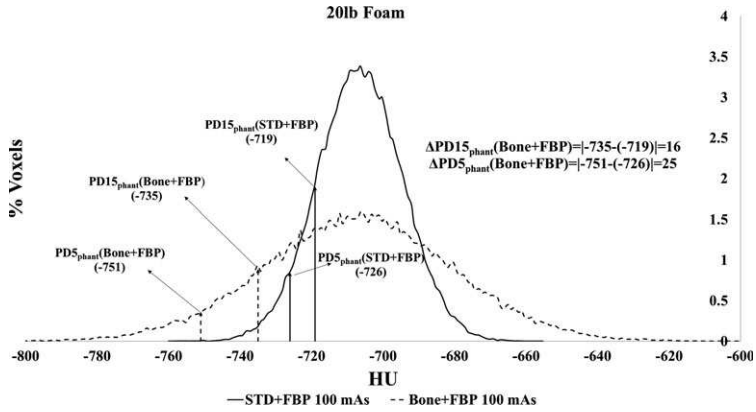

FIG. 4. A similar lung density histogram from a 20 lb reference foam embedded within the COPDGene 2 phantom showing a significant shift in PD15 and PD5 measures when using a Bone+FBP reconstruction scheme compared to the conventionally recommended STD+FBP reconstruction.

of lung densities differ for the two reconstructions by as much as 4.1% and 42 HU values, respectively. For purposes of analysis, we define histogram measures for the phantoms that are analogous to PD15 density measures in the lungs (Fig. 4) as $PD15_{phant}$. Specifically, foam HU values at a percent density of 5% of the histogram ($PD5_{phant}$) serve as quantitative comparators among different reconstructions and as an analog to PD15 and RA-950 since RA-950 in normal lungs is associated with the lowest 1–5% of the lung histogram.

The 5th and 15th percentiles of the histogram of CT numbers are normalized measures corresponding to the low-density "tail" of the density histogram for each material in the phantom. This enabled us to test whether quantitative metrics, as opposed to a qualitative assessment of density distributions, at both a conventional threshold (15%), and a more stringent threshold (5%) were consistent across all materials and reconstructions. To determine the values for $PD15_{phant}$ and $PD5_{phant}$, the cumulative distribution of voxel values was obtained using the measured histograms for each region and the HU value corresponding to the 5% and 15% thresholds of the calculated cumulative distribution. The difference from the recommended reconstruction method (STD-FBP) was reported as $\Delta PD15_{phant}$ and $\Delta PD5_{phant}$.

3. RESULTS

3.A. CT density measurements

Graphical and tabular results of measures of mean HU values, corresponding σ_{HU} values, and in all density standards are summarized in the appendix (Figures A1(a–g), and A2 (a–g) and Tables A1, A2, A3, A4, A5). Mean HU values of each of the reference density foams do not fluctuate significantly (mean HU $\leq$ 4) for different reconstructions or doses (Fig. 5). The small disparities in mean HU values that do

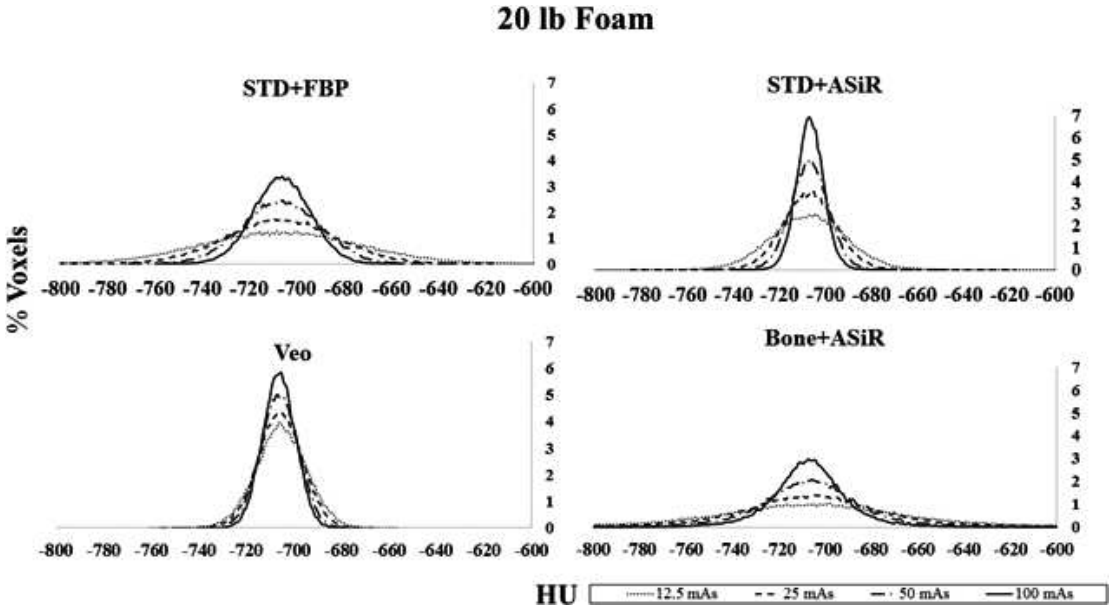

FIG. 5. Density histograms for the 20 lb density foam insert using various IR and kernel combinations. Note the similarity of the plots between the STD+FBP and Bone+ASiR reconstructions.

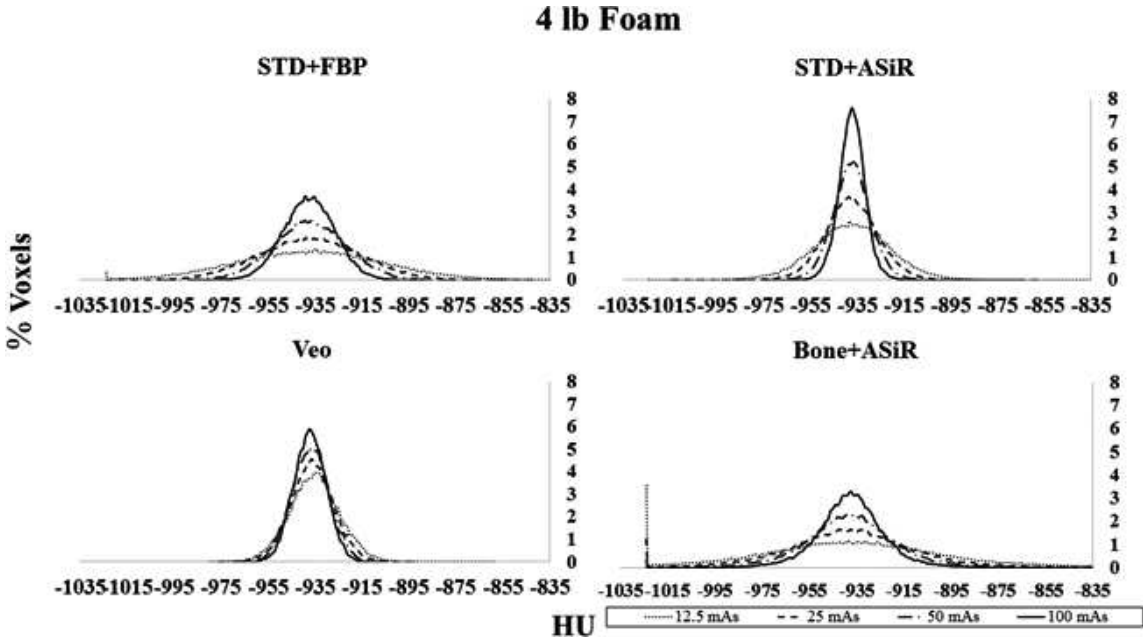

FIG. 6. Density histogram plots of each of the recons for the 4 lb foam using various IR and kernel combinations that show the same general trend as the 20 lb foam in Fig. 5.

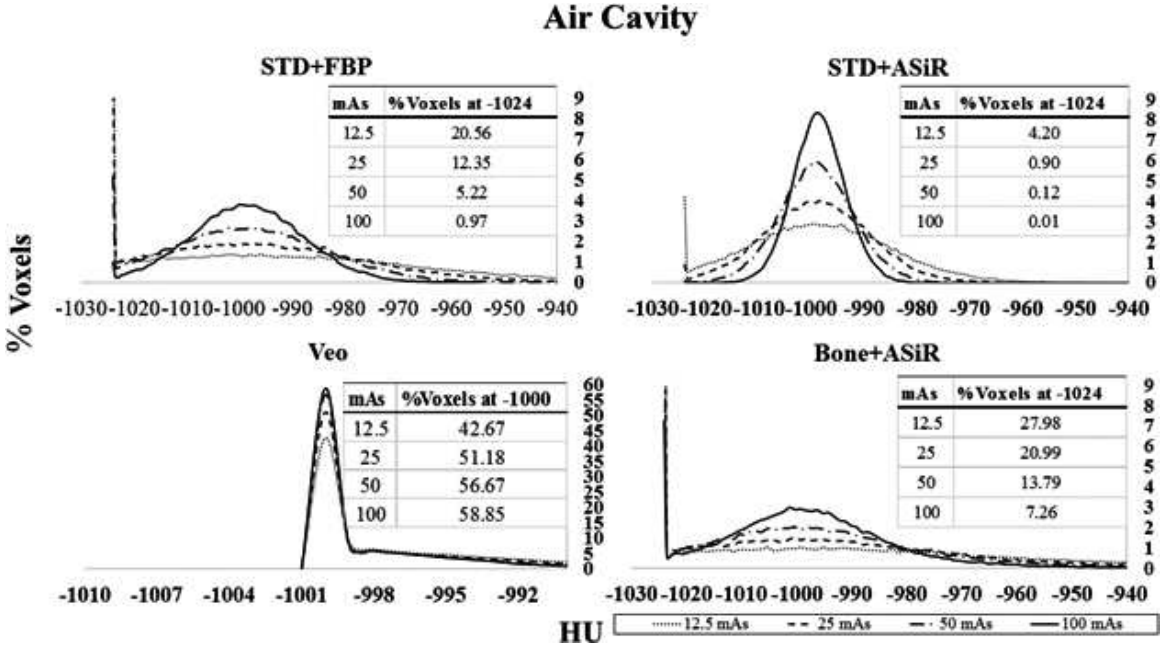

FIG. 7. Histograms of the air cavity of the COPDGene2 phantom with a corresponding table of the percentage of voxels at the −1024 value for each dose level and at −1000 for Veo. The −1024 HU truncation is most apparent in this region as is seen by the sudden peak in the distribution at the lower bound of the HU scale for all recons except Veo. The unusual histogram distribution of the Veo recon with an increase in peak value of the distribution of ~500% compared to the other recons is shown in the lower left plot.

exist are most prominent among the lower attenuating regions (Air and 4 lb. foam in Figs. 6 and 7). The primary source of these systematic errors is due to the truncation of the minimum range of HU reportable values. Presently, the CT system used in these studies truncates air densities and assigns CT number values to the minimum integer value in the range (−1024 in this case), which is readily apparent as a spike at this value in the density histograms. An exception to this explanation is the effect on the density histogram of the air cavity resulting from the Veo model-based IR where a similar pile-up in values occurs at −1000 HU suggesting a nonlinear mapping of air values to this value with obvious potential for concern when quantitative values are desired.

Note that the truncation artifact becomes more prominent in lower dose scans, as is shown in Fig. 7 with the exception of the Veo recon where the histogram becomes highly peaked

at −1000 HU. The truncation at the lowest HU values contributes to progressively increasing deviations in the mean and σ_{HU} in Table A1, as dose is decreased.

The sharply peaked histogram distribution of STD+ASiR and Veo algorithms qualitatively contrasts with the less peaked distributions of STD+FBP and Bone+ASiR and reflects a balance between noise amplification due to bandwidth of the kernel, Poisson noise due to varying CT dose, and noise mitigation by the ASiR or MBIR. For example, the similarity between plots of STD+FBP and Bone+ASiR is due to the balance of these processes and holds for various mAs dose settings as well as different material densities because the Bone+ASiR is less sharply peaked than those of IR recons with the lower bandwidth STD reconstruction kernel. Histograms of densities from the Bone+ASiR combination were fitted to model Gaussian distributions, and the standard deviation of the Gaussian model (denoted as σ) was derived for direct comparison with conventionally recommended STD+FBP histograms. The mean values of all the histograms are nearly identical as noted previously (Tables A1–A4), while σ varies markedly with acquired dose and reconstruction parameters. The results of this analysis are shown in Table II and graphically in Fig. 8. Overall, the σ values measured were most similar between the STD+FBP and the Bone+ASiR combination. Consequently, the discrepancy in $\Delta PD15_{phant}$ and $\Delta PD5_{phant}$ observed is negligible (Fig. 8 and Table A5) and largely a by-product of the truncation artifact already described. The $\Delta PD15_{phant}$ and $\Delta PD5_{phant}$ represent the differences between the threshold values obtained from density histograms derived from STD+ASiR, Veo, and Bone+ASiR recons to the STD+FBP recon as the reference standard. Consistent with the values of σ, all of the higher attenuating materials (20 lb foam, water, and acrylic), $\Delta PD15_{phant}$ and $\Delta PD5_{phant}$, were the smallest (~3 HU) for Bone+ASiR at all dose levels. This is in contrast to other IR and kernel combinations that varied by as much as ~45 HU deviation from STD+FBP (Table A5). For lower attenuating regions (12 lb foam, air, lung foam, and to lesser extent 4 lb foam), both $\Delta PD15_{phant}$ and $\Delta PD5_{phant}$ increase significantly likely due to the truncation artifact already noted. This is, in fact, another manifestation of the −1024 HU truncation artifact that drives the mean of the distribution in the positive direction.

TABLE II. A summary of the peak analysis performed by fitting Gaussian distribution curves to the data points of the two low attenuating materials to obtain the peak width (σ) together with the R-square goodness of fit to the Gaussian curve. σ is most similar between STD+FBP and Bone+ASiR, while IR only recons are about a factor of ~2 smaller in peak width.

Region	mAs	Recon	Peak width (σ)	R-square
VII (Lung foam)	12.5	FBP	42.98	0.997
		ASiR	19.84	0.999
		Veo	14.39	0.998
		Bone+ASiR	57.18	0.979
	25	FBP	29.89	0.998
		ASiR	13.73	0.998
		Veo	12.52	0.999
		Bone+ASiR	38.67	0.981
	50	FBP	20.90	0.997
		ASiR	9.65	0.999
		Veo	11.21	0.999
		Bone+ASiR	26.94	0.984
	100	FBP	14.23	0.997
		ASiR	6.64	0.999
		Veo	9.76	0.999
		Bone+ASiR	17.79	0.986
III (12 lb)	12.5	FBP	44.92	0.997
		ASiR	21.12	0.998
		Veo	14.16	0.998
		Bone+ASiR	59.31	0.960
	25	FBP	32.81	0.998
		ASiR	15.27	0.999
		Veo	12.57	0.999
		Bone+ASiR	41.97	0.984
	50	FBP	22.85	0.998
		ASiR	10.88	0.999
		Veo	11.02	0.999
		Bone+ASiR	29.62	0.986
	100	FBP	15.80	0.999
		ASiR	7.79	0.999
		Veo	9.88	0.999
		Bone+ASiR	19.94	0.989

4. DISCUSSION

This work demonstrates that IR, ASiR in this work, in combination with higher resolution kernels such as Bone, preserves the density histogram and qCT measures derived from density thresholds. The amplification of noise from lower dose and higher bandwidth kernels was balanced by the mitigation of noise achieved through IR. This finding supports previous work showing that the Bone+ASiR recon improves spatial resolution for quantitative airway measures. The finding that the same reconstruction approach does not significantly alter the density histogram invites further investigation of lower overall radiation dose protocols for lung CT quantification.[19] Ideally, a high-frequency qCT kernel could be defined that is common to each vendor platform and would enhance airway and maintain density measures in the lungs. Other acquisition and reconstruction parameters, such as slice thickness, display field of view, etc., can be optimized to refine the Bone+ASiR approach for density qCT using higher bandwidth kernels and IR techniques more generally. Feasibility to extend this technique to other manufacturers' platforms, such as the use of sharper kernels with Siemens' sinogram affirmed iterative reconstruction (SAFIRE) algorithm, an MBIR method, is necessary to confirm the approach can be widely disseminated for clinical research trials. Findings by Sieren et al. found similar behavior for SAFIRE on the Siemens platform (Siemens SOMATOM Definition Flash), which supports the possibility of similar behavior across these two major vendor platforms.[26] Indeed, Sieren et al. also found a nearly identical truncation artifact

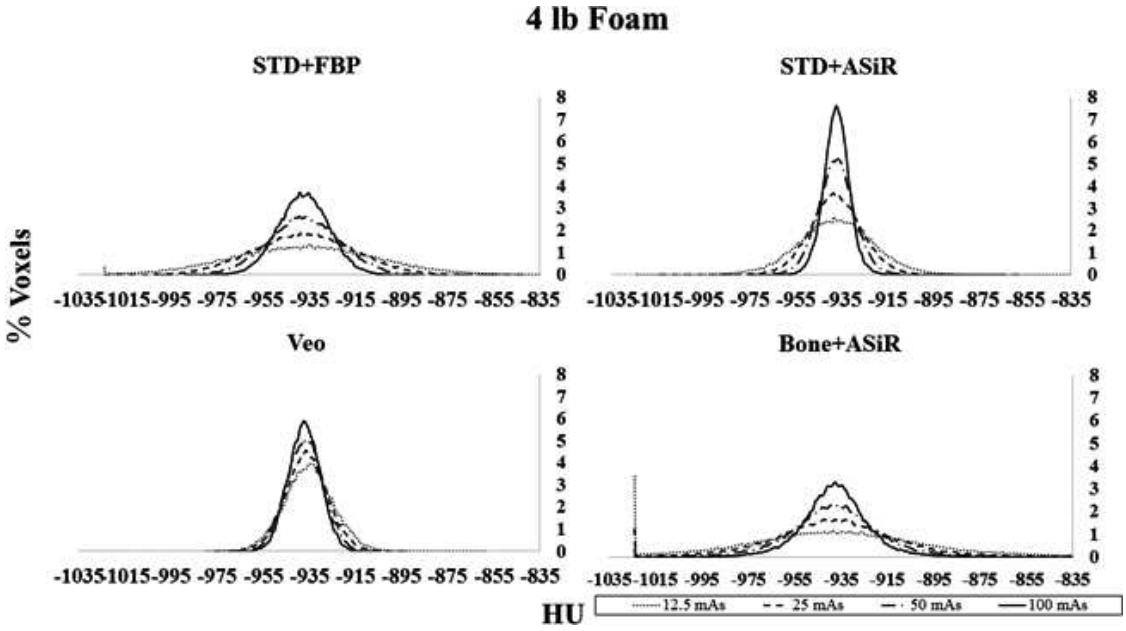

FIG. 8. Density histograms of the reference 4lb foam ("emphysema equivalent") insert in the COPDGene 2 phantom using various reconstruction parameters. Quantitatively and qualitatively the distribution of STD+FBP and Bone+ASiR are very similar.

at the low end of the density range on the Siemens SOMATOM Definition Flash system. For example, equivalent combinations of dose, kernel and IR for other vendors (Siemens' B75f+SAFIRE for instance), may also improve qCT of lung airways while preserving densitometry in the evaluation of progressive obstructive lung diseases and should be tested to confirm reproducibility of the results presented.

Second, the truncation artifact at −1024 clearly has significant effects on density measures in our experiments. Whether this has significant impact on the quantification of emphysema in human subjects in clinical research studies is an open question, but the truncation artifact is easily remedied by extending the lower limit of the HU reportable values by a few hundred HU. The HU scale should be carefully distinguished from the −1024 minimum reported value that was set long ago, likely for general computation reasons that no longer exist and could be easily fixed by the vendors. Importantly, this error will be amplified for lower patient dose protocols in qCT, because lower radiation dose will increase the number of voxels at the lower tail of the histogram exacerbating the truncation artifact.

Third, using ground truth density values in phantom experiments, we have shown that IR effects on the density histogram and quantification of emphysema in qCT of the lung based on density thresholds. The overall reduction in the standard deviation of the density histogram was observed across all radiation doses and material composition. While it is true that ASiR and Veo preserve mean HU values for each material, the impact of reduced standard deviation on histogram thresholds measured from the phantom may translate to a collective effect of skewing values measured in human scans since the overall histogram is effectively a summation of histogram of the materials within the volume. Additional confounding factors such as the inability to specify a reconstruction kernel and lengthy recon times (~45 min per series) for Veo suggest a cautious approach is needed when applying IR methods for qCT of the lung generally. A newer hybrid version of IR, not available on our scanner at the time of this study, called ASiR-V has been released by GE and may address these issues and should be investigated further. Nonetheless, our findings show a promising road forward using higher frequency reconstruction kernels with IR methods in combination.

This study does have several recognized limitations. First, although the COPDGene2 phantom is an extremely useful tool, the design and relative distribution of homogenous cylindrical materials are only an approximation to that of a human lung. The complexity of various structures such as vasculature and higher attenuating bone structures in the ribs, chest, and shoulders are not present in the phantom. Although the phantom is deficient in this aspect, it is worth stating that it does allow for separate investigation of material densities typically conglomerated in the lung in order to investigate the mechanisms that play a role in qCT on a material-by-material basis. From these investigations, extrapolation to more complex situations can be hypothesized and tested. The simple nature of the phantom also provides an equivalent platform to investigate extension of improved techniques found on one system to other various manufactures' CT scanners in order to possibly create cross platform compliance and quality assurance testing.[32] This same rationale can also be applied to lower dose protocols which take advantage of recon schemes suggested in this study. Another limitation is the constant evolution of IR algorithms as manufacturers advance new software versions commercially. Although these IR schemes may continue to evolve, the basic principles incorporated in these algorithms will likely not change drastically such that our general findings will remain a starting point for further refinement and optimization.

In summary, we found that the combined use of IR with higher resolution (Bone+ASiR) recon techniques shows promise for preserving qCT lung densitometry measurements by not significantly affecting density histograms in foams mimicking densities expected in lung parenchyma even at substantially reduced X-ray dose. The added benefit of this approach shown previously to improve accuracy of airway measures[19] strengthens the motivation and feasibility for investigation in human studies using this reconstruction approach. More generally, this study confirms that statistical and model-based IR methods differ with respect to their impact on quantitative density measures and must be implemented with a holistic approach to parameter selection to avoid variation and errors for histogram measures of lung densitometry. In its current form, the model-based IR method Veo (version 2.0) investigated here is limited in its flexibility for density measures; improved MBIR approaches such as ASiR-v may address these limitations inviting further study. Finally, the largest confounding factor in qCT of the lung densitometry in these studies stems from the arbitrary truncation of the of the integer representation of HU values at −1024 causing erroneous signal pile-up in the density histogram that can be easily remedied by extending the range of integer values below this limit.

ACKNOWLEDGMENTS

NIBIB-PB-EB-1010-159-JKS "Recovery – Quantitative Imaging Biomarker Alliance (QIBA)"; NIH/NHLBI U10 HL109168.

CONFLICT OF INTEREST

No conflict of interest or financial disclosures to report.

APPENDIX

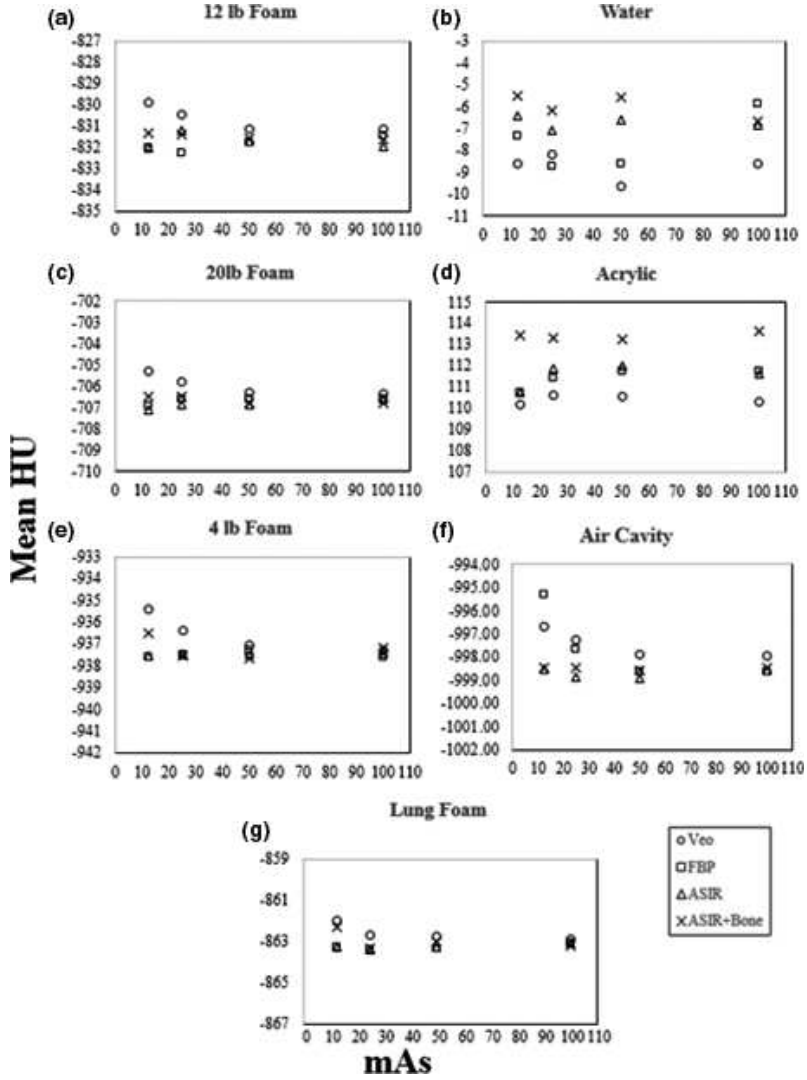

FIG. A1. Plots of the mean HU value dependence on tube current (and X-ray dose) for each of the materials in the COPDGene 2 phantom for (a) 12 lb foam, (b) water, (c) 20 lb foam, (d) acrylic, (e) 4 lb foam, (f) air cavity, and (g) lung foam. For lower density materials, the variation increases with lower mAs due in part to the truncation artifact.

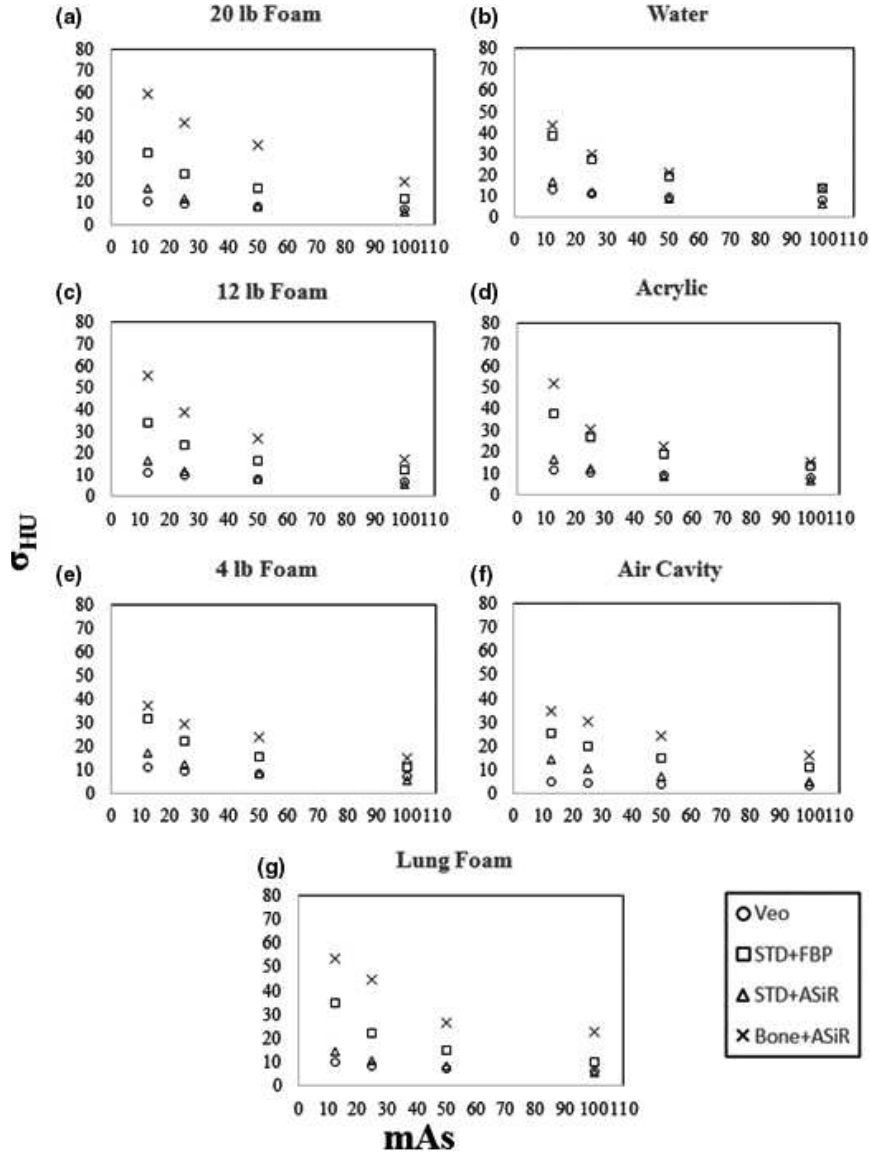

FIG. A2. Plots of the noise performance (σ_{HU}) with tube current (dose) for (a) 12 lb foam, (b) water, (c) 20 lb foam, (d) acrylic, (e) 4 lb foam, (f) air cavity, and (g) lung foam. Noise is highest for the Bone+ASiR reconstruction for each of the 7 regions within the phantom.

TABLE A1. The mean and SD of the measured HU using STD+FBP for mAs values of 100–12.5 mAs. For the air region, the effect of truncation at −1024 HU is most notable at 12.5 mAs which shifts the mean substantially in the positive direction by 4 HU.

STD+FBP				
Region	Mean HU ± SD			
mAs	100	50	25	12.5
I (20 lb)	−707 ± 12.01	−707 ± 16.62	−707 ± 23.91	−707 ± 33.83
II (Water)	−6 ± 13.86	−9 ± 19.10	−9 ± 27.12	−7 ± 38.39
III (12 lb)	−831 ± 11.48	−832 ± 16.18	−832 ± 23.10	−832 ± 32.30
IV (Acrylic)	112 ± 13.69	112 ± 19.14	111 ± 27.00	111 ± 38.05
V (4 lb)	−938 ± 10.94	−937 ± 15.63	−938 ± 22.13	−938 ± 31.34
VI (Air)	−999 ± 10.63	−999 ± 14.52	−998 ± 19.48	−995 ± 25.34
Lung foam	−863 ± 10.15	−863 ± 15.24	−863 ± 22.41	−863 ± 34.66

TABLE A2. The mean and SD of the measured HU using 100% ASiR. The truncation artifact mentioned previously does not a have a significant effect on ASiR recons due to the more sharply peak nature of the distribution of voxel values about the mean HU.

STD+ASiR				
Region	Mean HU ± SD			
mAs	100	50	25	12.5
I (20 lb)	−707 ± 5.73	−707 ± 8.13	−707 ± 11.88	−707 ± 16.70
II (Water)	−7 ± 6.37	−7 ± 8.59	−7 ± 12.18	−6 ± 17.10
III (12 lb)	−832 ± 5.72	−832 ± 8.10	−831 ± 11.79	−832 ± 16.31
IV (Acrylic)	112 ± 6.76	112 ± 8.88	112 ± 12.08	111 ± 16.77
V (4 lb)	−937 ± 5.54	−938 ± 8.19	−938 ± 11.83	−938 ± 16.79
VI (Air)	−999 ± 5.02	−999 ± 7.24	−999 ± 10.29	−999 ± 14.07
Lung foam	−863 ± 5.89	−863 ± 8.26	−863 ± 10.59	−863 ± 14.64

TABLE A3. The mean and SD of the measured HU using the combination of 100% ASiR with the bone kernel. The overall fluctuation of the mean HU for all materials was very stable at ≤ 1 HU.

Bone+ASiR				
Region	Mean HU ± SD			
mAs	100	50	25	12.5
I (20 lb)	−707 ± 17.15	−707 ± 26.84	−707 ± 38.94	−707 ± 55.52
II (Water)	−7 ± 13.88	−6 ± 21.21	−6 ± 30.15	−6 ± 43.49
III (12 lb)	−832 ± 19.27	−832 ± 35.96	−831 ± 46.56	−831 ± 59.41
IV (Acrylic)	114 ± 15.27	113 ± 22.63	113 ± 30.6	113 ± 51.69
V (4 lb)	−937 ± 14.88	−938 ± 23.63	−938 ± 29.51	−937 ± 37.16
VI (Air)	−998 ± 16.13	−997 ± 24.28	−998 ± 30.47	−998 ± 34.47
Lung foam	−863 ± 22.86	−863 ± 26.45	−863 ± 44.9	−862 ± 53.4

TABLE A4. The mean and SD of the measured HU using the combination of the model-based iterative reconstruction algorithm, Veo. In all cases, the noise of the image remained relatively stable even at a fourth of the mAs.

Veo				
Region	Mean HU ± SD			
mAs	100	50	25	12.5
I (20 lb)	−706 ± 7.00	−706 ± 8.20	−706 ± 9.79	−705 ± 11.22
II (Water)	−9 ± 8.20	−10 ± 9.46	−8 ± 11.22	−9 ± 13.06
III (12 lb)	−831 ± 6.85	−831 ± 7.9	−830 ± 9.07	−830 ± 10.29
IV (Acrylic)	110 ± 8.05	111 ± 9.50	111 ± 10.64	110 ± 11.97
V (4 lb)	−937 ± 6.85	−937 ± 8.12	−936 ± 9.39	−935 ± 10.79
VI (Air)	−998 ± 3.05	−998 ± 3.45	−997 ± 4.19	−997 ± 4.88
Lung foam	−863 ± 6.13	−863 ± 7.43	−863 ± 8.61	−862 ± 10.30

TABLE A5. A summary of the measures of $\Delta PD15_{phant}$ and $\Delta PD5_{phant}$ for all regions. Note that the Bone+ASiR recon measures are smallest among most of the materials (regions I, II, IV, and V). The previously described HU scale truncation artifact causes values for low attenuating regions (III, VII) which increase $\Delta PD15_{phant}$ and $\Delta PD5_{phant}$ values artificially for Bone+ASiR.

Region	mAs	Recon	$\Delta PD5_{phant}$ (HU)	$\Delta PD15_{phant}$ (HU)	Δmean HU
I (20 lb)	12.5	ASiR	27	17	0.17
		Veo	45	18	1.64
		Bone+ASiR	6	2	0.42
	25	ASiR	25	5	0.25
		Veo	23	16	0.81
		Bone+ASiR	21	8	0.07
	50	ASiR	13	9	0.27
		Veo	14	9	0.29
		Bone+ASiR	1	2	0.20
	100	ASiR	21	6	0.00
		Veo	20	5	0.26
		Bone+ASiR	3	3	0.15
II (Water)	12.5	ASiR	36	22	0.94
		Veo	40	25	1.23
		Bone+ASiR	6	1	1.84
	25	ASiR	26	17	1.65
		Veo	27	17	0.52
		Bone+ASiR	3	1	2.53
	50	ASiR	20	12	2.01
		Veo	16	9	1.02
		Bone+ASiR	1	1	3.04
	100	ASiR	10	7	1.01
		Veo	6	3	2.73
		Bone+ASiR	4	1	0.81
III (12 lb)	12.5	ASiR	27	17	0.03
		Veo	38	25	2.11
		Bone+ASiR	47	18	0.66
	25	ASiR	21	14	1.07
		Veo	25	17	1.82
		Bone+ASiR	31	10	0.91
	50	ASiR	14	9	0.05
		Veo	15	10	0.63
		Bone+ASiR	23	8	0.19
	100	ASiR	9	5	0.47
		Veo	8	4	0.35
		Bone+ASiR	15	6	0.16
IV (Acrylic)	12.5	ASiR	36	23	0.00
		Veo	42	27	0.58
		Bone+ASiR	10	1	2.68
	25	ASiR	30	19	0.42
		Veo	25	16	0.79
		Bone+ASiR	6	0	1.89
	50	ASiR	16	10	0.22
		Veo	15	9	1.20
		Bone+ASiR	4	1	1.51
	100	ASiR	11	7	0.15
		Veo	7	4	1.48
		Bone+ASiR	2	1	1.84

TABLE A5. Continued.

Region	mAs	Recon	$\Delta PD5_{phant}$ (HU)	$\Delta PD15_{phant}$ (HU)	Δmean HU
V (4 lb)	12.5	ASiR	25	16	0.06
		Veo	37	24	2.19
		Bone+ASiR	22	9	1.05
	25	ASiR	18	11	0.02
		Veo	22	14	1.07
		Bone+ASiR	15	6	0.06
	50	ASiR	12	8	0.21
		Veo	13	9	0.23
		Bone+ASiR	10	3	0.41
	100	ASiR	9	6	0.19
		Veo	7	4	0.28
		Bone+ASiR	7	3	0.44
VI (Air)	12.5	ASiR	1	10	3.22
		Veo	23	23	1.40
		Bone+ASiR	0	0	6.77
	25	ASiR	8	14	1.24
		Veo	23	23	0.37
		Bone+ASiR	0	9	3.93
	50	ASiR	13	18	0.32
		Veo	23	23	0.75
		Bone+ASiR	0	2	1.99
	100	ASiR	9	6	0.05
		Veo	15	9	0.65
		Bone+ASiR	8	5	0.83
VII (Lung foam)	12.5	ASiR	27	18	0.01
		Veo	35	23	1.28
		Bone+ASiR	44	17	0.95
	25	ASiR	18	12	0.01
		Veo	21	14	0.72
		Bone+ASiR	31	12	0.05
	50	ASiR	13	8	0.02
		Veo	13	8	0.57
		Bone+ASiR	21	8	0.30
	100	ASiR	9	6	0.01
		Veo	7	4	0.22
		Bone+ASiR	13	5	0.10

[a]Author to whom correspondence should be addressed. Electronic mail. sfain@wisc.edu.

REFERENCES

1. Sieren J, Newell J Jr, Judy P, et al. Reference standard and statistical model for intersite and temporal comparisons of CT attenuation in a multicenter quantitative lung study. *Med Phys*. 2012;39:5757–5767.
2. Gietema HA, Müller NL, Fauerbach PVN, et al., E.o.C.L.t.I.P.S.E. investigators. Quantifying the extent of emphysema: factors associated with radiologists' estimations and quantitative indices of emphysema severity using the ECLIPSE cohort. *Acad Radiol*. 2011;18:661–671.
3. Grydeland TB, Dirksen A, Coxson HO, et al. Quantitative computed tomography measures of emphysema and airway wall thickness are related to respiratory symptoms. *Am J Respir Crit Care Med*. 2010;181:353–359.
4. Zach JA, Newell JD Jr, Schroeder J, et al. Quantitative CT of the lungs and airways in healthy non-smoking adults. *Invest Radiol*. 2012; 47:596.
5. Barr CCWGRG, Berkowitz EA, Bigazzi F, et al. A combined pulmonary-radiology workshop for visual evaluation of COPD: study design, chest CT findings and concordance with quantitative evaluation. *COPD*. 2012;9:151–159.
6. Han MK, Agusti A, Calverley PM, et al. Chronic obstructive pulmonary disease phenotypes: the future of COPD. *Am J Respir Crit Care Med*. 2010;182:598–604.
7. Han MK, Muellerova H, Curran-Everett D, et al. GOLD 2011 disease severity classification in COPDGene: a prospective cohort study. *Lancet Respir Med*. 2013;1:43–50.
8. Kim V, Davey A, Comellas AP, et al. Clinical and computed tomographic predictors of chronic bronchitis in COPD: a cross sectional analysis of the COPDGene study. *Respir Res*. 2014;15:52.
9. Regan EA, Hokanson JE, Murphy JR, et al. Genetic epidemiology of COPD (COPDGene) study design. *COPD*. 2011;7:32–43.
10. Dirksen A. Monitoring the progress of emphysema by repeat computed tomography scans with focus on noise reduction. *Proc Am Thorac Soc*. 2008;5:925–928.
11. Madani A, Maertelaer VD, Zanen J, Gevenois PA. Pulmonary emphysema: radiation dose and section thickness at multidetector CT

quantification—Comparison with macroscopic and microscopic morphometry. *Radiology*. 2007;243:250–257.
12. Lynch DA, Al-Qaisi ML. Quantitative CT in COPD. *J Thorac Imaging*. 2013;28:284.
13. Washko GR, Dransfield MT, Estepar RSJ, et al. Airway wall attenuation: a biomarker of airway disease in subjects with COPD. *J Appl Physiol*. 2009;107:185–191.
14. Aysola RS, Hoffman EA, Gierada D, et al. Airway remodeling measured by multidetector CT is increased in severe asthma and correlates with pathology. *CHEST J*. 2008;134:1183–1191.
15. Castro M, Fain SB, Hoffman EA, Gierada DS, Erzurum SC, Wenzel S, National Heart Lung & Blood Institute. Lung imaging in asthmatic patients: the picture is clearer. *J Allergy Clin Immunol*. 2011;128:467–478.
16. Brenner DJ, Hall EJ. Computed tomography—an increasing source of radiation exposure. *N Engl J Med*. 2007;357:2277–2284.
17. Gierada DS, Bierhals AJ, Choong CK, et al. Effects of CT section thickness and reconstruction kernel on emphysema quantification: relationship to the magnitude of the CT emphysema index. *Acad Radiol*. 2010;17:146–156.
18. Kemerink GJ, Kruize HH, Lamers RJ, van Engelshoven JM. CT lung densitometry: dependence of CT number histograms on sample volume and consequences for scan protocol comparability. *J Comput Assist Tomogr*. 1997;21:948–954.
19. Rodriguez A, Ranallo F, Judy P, Gierada D, Fain S. CT reconstruction techniques for improved accuracy of lung CT airway measurement. *Med Phys*. 2014;41:111911.
20. Salito C, Woods JC, Aliverti A. Influence of CT reconstruction settings on extremely low attenuation values for specific gas volume calculation in severe emphysema. *Acad Radiol*. 2011;18:1277–1284.
21. Shaker S, Dirksen A, Laursen L, et al. Short-term reproducibility of computed tomography-based lung density measurements in alpha-1 antitrypsin deficiency and smokers with emphysema. *Acta Radiol*. 2004;45:424–430.
22. Choo JY, Goo JM, Lee CH, Park CM, Park SJ, Shim M-S. Quantitative analysis of emphysema and airway measurements according to iterative reconstruction algorithms: comparison of filtered back projection, adaptive statistical iterative reconstruction and model-based iterative reconstruction. *Eur Radiol*. 2014;24:799–806.
23. Lee Y, Jin KN, Lee NK. Low-dose computed tomography of the chest using iterative reconstruction versus filtered back projection: comparison of image quality. *J Comput Assist Tomogr*. 2012;36:512–517.
24. Liu L. Model-based iterative reconstruction: a promising algorithm for today's computed tomography imaging. *J Med Imaging Radiat Sci*. 2014;45:131–136.
25. Silva AC, Lawder HJ, Hara A, Kujak J, Pavlicek W. Innovations in CT dose reduction strategy: application of the adaptive statistical iterative reconstruction algorithm. *Am J Roentgenol*. 2010;194:191–199.
26. Sieren J, Hoffman E, Fuld M, Chan K, Guo J, Newell J Jr. Sinogram affirmed iterative reconstruction (SAFIRE) versus weighted filtered back projection (WFBP) effects on quantitative measure in the COPDGene 2 test object. *Med Phys*. 2014;41:091910.
27. Hague CJ, Krowchuk N, Alhassan D, et al. Qualitative and quantitative assessment of smoking-related lung disease: effect of iterative reconstruction on low-dose computed tomographic examinations. *J Thorac Imaging*. 2014;29:350–356.
28. Mets OM, Willemink MJ, de Kort FP, et al. The effect of iterative reconstruction on computed tomography assessment of emphysema, air trapping and airway dimensions. *Eur Radiol*. 2012;22:2103–2109.
29. Jarjour NN, Erzurum SC, Bleecker ER, et al. Severe asthma: lessons learned from the national heart, lung, and blood institute severe asthma research program. *Am J Respir Crit Care Med*. 2012;185:356–362.
30. Li G, Liu X, Dodge CT, Jensen CT, Rong XJ. A noise power spectrum study of a new model-based iterative reconstruction system: Veo 3.0. *J Appl Clin Med Phys*. 2016;17:1–12.
31. Fedorov A, Beichel R, Kalpathy-Cramer J, et al. 3D Slicer as an image computing platform for the quantitative imaging network. *Magn Reson Imaging*. 2012;30:1323–1341.
32. Judy P, Estepar RSJ, Hoffman E, Lynch D. SU-FF-I-06: COPDGene study quality assurance phantom. *Med Phys*. 2009;36:2435.